Applied Energy 140 (2015) 365–377

Contents lists available at ScienceDirect

Applied Energy

journal homepage: www.elsevier.com/locate/apenergy

A comparison of electric power output of CO_2 Plume Geothermal (CPG) and brine geothermal systems for varying reservoir conditions

Benjamin M. Adams [a], Thomas H. Kuehn [a,*], Jeffrey M. Bielicki [b,c], Jimmy B. Randolph [d], Martin O. Saar [d,e]

[a] Department of Mechanical Engineering, University of Minnesota, 111 Church St SE, Minneapolis, MN 55455, USA
[b] Department of Civil, Environmental, and Geodetic Engineering, The Ohio State University, 2070 Neil Avenue, Columbus, OH 43210, USA
[c] John Glenn School of Public Affairs, The Ohio State University, 1810 College Road, Columbus, OH 43210, USA
[d] Department of Earth Sciences, University of Minnesota, 310 Pillsbury Drive SE, Minneapolis, MN 55455, USA
[e] Department of Earth Sciences, ETH-Zürich, Sonneggstrasse 5, 8092 Zürich, Switzerland

HIGHLIGHTS

- CO_2 has less pressure losses in a sedimentary geothermal reservoir than brine.
- CO_2 produces more power at shallower depths and lower permeabilities than brine.
- CO_2 is a better working fluid in secondary Rankine cycles than R245fa.
- Increasing the well diameters dramatically increases geothermal power production.

ARTICLE INFO

Article history:
Received 22 July 2014
Received in revised form 12 November 2014
Accepted 20 November 2014
Available online 20 December 2014

Keywords:
Carbon dioxide
Geothermal energy
Carbon dioxide utilization
Renewable energy
Carbon dioxide plume
Working fluid

ABSTRACT

In contrast to conventional hydrothermal systems or enhanced geothermal systems, CO_2 Plume Geothermal (CPG) systems generate electricity by using CO_2 that has been geothermally heated due to sequestration in a sedimentary basin. Four CPG and two brine-based geothermal systems are modeled to estimate their power production for sedimentary basin reservoir depths between 1 and 5 km, geothermal temperature gradients from 20 to 50 °C km^{-1}, reservoir permeabilities from 1×10^{-15} to 1×10^{-12} m^2 and well casing inner diameters from 0.14 m to 0.41 m. Results show that CPG direct-type systems produce more electricity than brine-based geothermal systems at depths between 2 and 3 km, and at permeabilities between 10^{-14} and 10^{-13} m^2, often by a factor of two. This better performance of CPG is due to the low kinematic viscosity of CO_2, relative to brine at those depths, and the strong thermosiphon effect generated by CO_2. When CO_2 is used instead of R245fa as the secondary working fluid in an organic Rankine cycle (ORC), the power production of both the CPG and the brine–reservoir system increases substantially; for example, by 22% and 20% for subsurface brine and CO_2 systems, respectively, with a 35 °C km^{-1} thermal gradient, 0.27 m production and 0.41 m injection well diameters, and 5×10^{-14} m^2 reservoir permeability.

1. Introduction

In the United States, the Earth's crust contains an estimated 200,000 exajoules of extractable thermal energy—approximately 2000 times the current U.S. annual primary energy consumption—of which an estimated 100 GWe of geothermal energy could be added within the next 50 years [1]. Currently, the United States has an installed geothermal power production capacity of 3.4 GWe, mostly in California and Nevada, which utilize high geothermal temperature gradients and shallow fracture networks within the subsurface [2]. As a consequence, technologies must be developed to more efficiently utilize undeveloped geothermal resources, such as high-temperature but lower-permeability reservoirs, or high-permeability but cooler reservoirs. Enhanced Geothermal Systems (EGS) can be deployed in high-temperature/low-permeability resources to increase the power production of a system by fracturing deep (typically about 5 km) crystalline basement rock to increase its permeability [3], but EGS is controversial (e.g., [4]). This paper describes an approach which does not require fracturing because it utilizes relatively shallow (1–5 km), low-temperature, naturally high-permeability sedimentary or stratigraphic reservoirs that are overlain by a low-permeability caprock. We calculate the electric power that could be produced from these geologic

* Corresponding author.
E-mail address: kuehn001@umn.edu (T.H. Kuehn).

http://dx.doi.org/10.1016/j.apenergy.2014.11.043
0306-2619/

layers by using CO_2 as the subsurface heat extraction fluid and compare the results with traditional brine-based electric power production from such reservoirs.

CO_2 was first proposed as a geothermal working fluid in EGS only [5,6]. CO_2 has two primary advantages over brine: (1) it has a low kinematic viscosity, allowing for effective heat advection; and (2) the density of CO_2 varies much more with temperature than that of brine which generates a stronger thermosiphon through the injection and production wells, that can thus reduce or eliminate the need for pumps circulating the subsurface fluid through the reservoir [23,24,7]. Additionally, employing CO_2 as the heat extraction fluid can result in diminished fluid–mineral reactions, restricted to a relatively small region that will migrate as the CO_2 plume grows [8,9].

CO_2 Plume Geothermal (CPG) differs from using CO_2 in EGS [5,6] because CPG extracts heat from naturally permeable, sedimentary or stratigraphic basins [10–12]. These sedimentary basins have larger contacting surfaces which make them favorable for heat exchange using CO_2 [13]. These geologic formations are common throughout the United States and the world [14]; for example, they exist below approximately half of North America [15,16] where economically favorable sequestration sites have been identified [17]. Such sedimentary basins have been used for CO_2 disposal in some parts of the world, including one project that began in the mid-1990s [18] and are the target of current CO_2 capture and sequestration (CCS) efforts [19] to reduce global climate change [14]. Therefore, coupling CPG with an existing CO_2 sequestration project—thus creating a CO_2 capture utilization and sequestration (CCUS) process—can reduce the costs of sequestration by using CO_2 as a resource to generate electricity [20,21] and distributes the cost of subsurface exploration over multiple activities [22].

To date, research into electric power production, using CO_2 as the subsurface working fluid, has primarily focused on EGS reservoirs at a limited set of conditions [23–25,3]. Atrens [24] calculated exergy production (largest theoretical surface plant electric power production) for both subsurface CO_2 and water for a single set of parameters: a 225 °C, 5 km, fixed-permeability reservoir modeled with the Darcy equation, and 0.23 m injection and production well diameters. Beckers et al. [3] calculated electric power production and Levelized Cost of Electricity (LCOE) for EGS with fixed mass flowrates by varying multiple parameters including depth, geothermal temperature gradient, well diameter, and surface plant design.

To date, CPG research has focused on reservoir and wellbore fluid dynamics. Randolph and Saar [11,26] presented initial estimates of electrical power production using a simple Carnot-based power plant and a fixed mass flowrate, depth, and temperature. Buscheck et al. [27] found that active reservoir management—the manipulation of reservoir characteristics such as plume size or pressure—is necessary to maintain power production after initial CPG deployment. Buscheck et al. [28] extended the reservoir modeling to use both CO_2 and brine as geothermal working fluids, but focused on the engineered pressure gradients between concentric rings of CO_2 and brine wells, and used a simple model to predict CO_2 power production. Janke and Kuehn [29] primarily modeled the surface plant and power production of a CPG system, using a fixed pressure drop reservoir. Despite the fixed mass flowrate of 70 kg s^{-1}, for a 2.5 km, 100 °C geothermal reservoir, they showed that directly expanding the CO_2 through a turbine (direct system) produces 2×–8× more power than a secondary Rankine cycle (indirect system). Direct CO_2-based geothermal power cycles can have higher cycle efficiencies, but they are not yet commercially available. Some effort is being made to adapt existing waste heat recovery turbomachinery to generate electricity from produced CO_2 at a CCUS demonstration site at Cranfield, MS, USA [63].

One advantage of using CO_2 as a geologic working fluid is the substantial mass flowrates obtained from the density-driven thermosiphon [7]. These authors combined a reservoir model with wellbore and surface piping models to estimate the strength of this thermosiphon for several depths and temperature gradients and showed substantial mass flowrates at depths as shallow as 1 km. Similarly, Pan et al. [30] used a multi-phase, multi-fluid wellbore simulator, T2Well, coupled with a reservoir model to show the strength of the thermosiphon for a 3 km, 152 °C pure-CO_2 sedimentary reservoir with a 10^{-13} m^2 permeability, using industry-standard 4 in. (0.1 m) and 7 in. (0.18 m) piping. While Pan et al. [30] fix mass flowrate, they show, by way of a pressure differential between injection and production wellheads, that a thermosiphon will be established.

In this paper, we expand upon our previous work by coupling combined fluid-dynamic-thermodynamic models of sedimentary basin reservoirs with models of injection/production wells and the surface plant, for varying reservoir conditions, piping, and surface plant configurations, in order to compare the performance of CPG and brine geothermal systems. Compared to previous studies, we investigate a much-expanded range of parameters (e.g. well diameters from 0.14 to 0.41 m) so as not to exclude any potentially profitable, and technologically possible, CPG configurations. For example, considering significantly larger, yet reasonable, well diameters is particularly important, given that pressure losses in the well are inversely proportional to the fifth power of the well diameter, thereby considerably affecting the power production of CPG and other geothermal systems. Additionally, unlike previous work, we do not parameterize mass flowrate, but instead operate at mass flowrates which provide maximum power generation.

In total, we model six sedimentary basin geothermal power plant scenarios (Table 1): (1) a direct CO_2 plant relying on the thermosiphon effect [7] to provide the CO_2 circulation through the geothermal reservoir and the surface plant; (2) a direct CO_2 plant with supplemental pumping; two indirect CO_2 plants using either (3) R245fa (1,1,1,3,3-Pentafluoropropane) or (4) CO_2 (R744) as the secondary working fluid; and two indirect brine plants using either (5) R245fa or (6) CO_2 as the secondary working fluid. For each scenario, the power production is calculated for reservoir depths of 1–5 km, geothermal temperature gradients of 20, 35, and 50 °C km^{-1}, reservoir permeabilities from 10^{-15} to 10^{-12} m^2, and well inner diameters from 0.14 to 0.41 m.

2. Methods

Each inverted 5-spot system configuration involves four major components: a reservoir, an injection well (IW), four production wells (PW), and a surface power plant (SYSTEM), as shown in Fig. 1. The CO_2-based systems are initially coupled with a CO_2 emitter to inject and fill the reservoir, but no such CO_2 sequestration and brine displacement are explicitly simulated. Instead, the

Table 1
Model parameters for six combinations of geothermal reservoir and power plant scenarios as described in the main text.

Power system	Direct CO_2 – thermosiphon only Direct CO_2 – supplemental pumping Indirect CO_2 – R245fa or CO_2 secondary Indirect brine – R245fa or CO_2 secondary
Well diameter (m)	0.14, 0.27, 0.33, and/or 0.41
Reservoir conditions	
Depth (km)	1.0, 1.5, 2.5, 3.5, or 5.0
Thermal gradient (°C km^{-1})	20, 35, or 50
Permeability	1×10^{-12} m^2 to 1×10^{-15} m^2

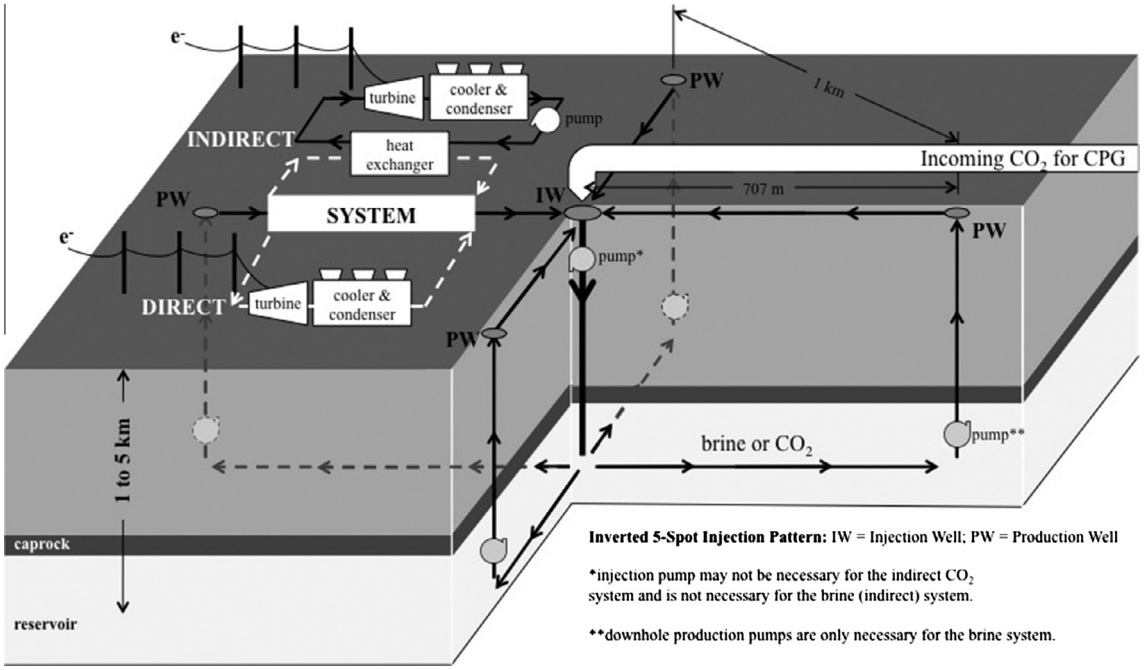

Fig. 1. Simplified system schematic showing geothermal reservoir, surface power plant system, and inverted 5-spot well pattern.

pore space of CPG reservoirs is assumed to be completely filled with CO_2. Total system performance is modeled by using two software packages: (1) TOUGH2 [31], with the Equation of State (ECO2N) module [31,32], is used for subsurface fluid and thermodynamic modeling of geothermal heat and fluid extraction as well as fluid re-injection into the reservoir; and (2) Engineering Equation Solver (EES) is used to simulate the surface plant power production and wellbore fluid flow. EES is a simultaneous equation solver with built-in thermodynamic property data, including data for CO_2 from Span and Wagner [33]. Model parameters are given in Table 2.

2.1. Base-case parameters

It is useful to select "base case" conditions to which various alternative options can be compared. Base case parameters include: a horizontal, homogeneous, isotropic reservoir with a thickness of 305 m at an average depth of 2.5 km, a porosity of 10%, and a permeability of 5×10^{-14} m^2 which is overlain by an impermeable caprock, a geothermal temperature gradient of 35 °C km^{-1} with an ambient air temperature of 15 °C, an injection well inner diameter of 0.41 m, and a production well inner diameter of 0.27 m. The geothermal temperature gradient is approximately the average value for the continental crust of the western United States of 34 °C km^{-1} [64,34]. The permeability of 5×10^{-14} m^2 is approximately the average horizontal permeability of sedimentary reservoirs: the Mt. Simon formation, into which 0.3 Mt CO_2 yr^{-1} is currently being sequestered near Decatur, Illinois [35], has an average horizontal permeability of 2.6×10^{-14} m^2 [36]; similarly, a larger study of the Illinois Basin reported typical average horizontal permeabilities between 3×10^{-14} and 10×10^{-14} m^2 [37,10]. The ambient air temperature assumed is 15 °C and is thus greater than most averages within the United States and represents the approximate average annual air temperature in Dallas, Texas. Because power production increases as ambient air temperature (thermodynamic heat sink) decreases, the power production found, when using a high average annual ambient air temperature of 15 °C, is a conservative, i.e., low, estimate of the expected average yearly power production (Section S4.3, Supplemental information).

2.2. Conceptual and numerical geologic model

The fluid injection and production pattern used in the present simulations is the standard inverted 5-spot configuration used in previous publications (e.g., [38,6,11]) with four symmetrically placed production wells, located at the corners of a 1 km by 1 km square (in map-view), and one injection well in the center (Fig. 1). This configuration allows direct comparison with previous publications although other well configurations, including horizontal production wells [39] will likely further improve system performance. The symmetrical layout of the inverted 5-spot well configuration and reservoir requires only one-eighth of the reservoir be modeled.

To facilitate direct comparison between brine and CO_2 geothermal systems, the pores are assumed to be completely filled with either pure CO_2 or 20 wt% NaCl brine. As a consequence, time-dependent behavior such as brine displacement by CO_2, heat depletion in the geothermal reservoir, or CO_2 dissolution into brine is not considered [40,39,41], and localized clogging due to salt precipitation has been remedied [42]. Reservoir parameters are described in Table 2. Reservoir boundary conditions include no fluid flow through over- and underlying (assumed) zero-permeability cap- and bedrocks and no flow due to lateral symmetry to adjacent inverted 5-spot well patterns as described in Oldenburg et al. [43], Pruess [6], and Randolph and Saar [11]. Heat transfer from over- and underlying formations is simulated with a standard semi-analytic conductive heat exchange boundary condition [44], while no heat transfer occurs at the lateral boundaries due to the aforementioned symmetry. All reservoir rock and fluid temperatures are initially uniform and are determined by the product of depth and geothermal gradient added to the ambient mean annual near-surface air temperature.

The state of the fluid produced from the reservoir depends on several factors, including reservoir depth, temperature, permeability, fluid mass flowrate, injection pressure, and injection temperature. These factors are determined by the system as a whole;

Table 2
Model parameters (as justified in the main text).

Primary system (reservoir) fluids	– 100% CO_2 – 20 wt% H_2O–NaCl (brine)
Secondary (ORC) system fluids (for indirect systems)	– CO_2 (R744) – 1,1,1,3,3-Pentafluoropropane (R245fa)
Downhole production well pressure	Hydrostatic
Direct turbine isentropic efficiency	78%
ORC turbine efficiency	80%
Pump efficiencies	90%
Well pipe material	Bare CR13
Well pipe roughness	55 μm [66]
Condensing or cooling tower approach temperature	7 °C (Section S4.2 of the Supplemental information)
Ambient mean annual air temperature	15 °C (Dallas, TX)
Reservoir constants	
Well configuration	Inverted 5-spot (over a 1 km^2 footprint, see Fig. 1)
Reservoir thickness and depth	305 m thick, 1–5 km deep (base case: 2.5 km deep)
Rock density	2300 kg m^{-3}
Reservoir porosity	0.10
Reservoir permeability	5×10^{-14} m^2 (base case only)
Reservoir volume	2.7×10^8 m^3
Reservoir fluid volume	0.3×10^8 m^3 (8.2 MMt CO_2 @ 2.5 km)
Initial reservoir temperature profile	Uniform
Lateral reservoir boundary condition	No heat or fluid flow
Vertical reservoir boundary condition	No fluid flow; heat conduction using TOUGH2 semi-analytic model [44]

therefore, the TOUGH2 reservoir model must be solved simultaneously with the well and surface power plant models. For a given reservoir at a fixed temperature and depth, the pressure change between injection and production wells tends to vary primarily with mass flowrate; we can thus describe the TOUGH2 reservoir model performance in terms of mass flowrate for every reservoir parameter combination, and use this characterization, along with produced fluid temperatures, in the well and surface power plant models.

For steady, laminar 1D flow through a porous medium, the pressure drop, ΔP, can be calculated using Darcy's Law [45], given by Eq. (1). For a specified reservoir at a given depth and temperature, the average fluid density, ρ, and dynamic viscosity, μ, are nearly constant. Likewise, the combination of reservoir properties length, L, and area, A, is constant. The combination of these four terms, referred to hereafter as the Average Specific Kinematic Viscosity, S, is contained in brackets in Eq. (1). When the value of S is divided by reservoir permeability, κ, it represents a constant of proportionality, $R = S/\kappa$, relating ΔP to fluid mass flowrate, $\dot{m}$.

$$\Delta P = \left[\frac{\mu L}{\rho A}\right]\frac{\dot{m}}{\kappa} = S\frac{\dot{m}}{\kappa} = R\dot{m} \tag{1}$$

Thus, R may be viewed as a "reservoir parameter" that combines both fluid and porous medium properties, similar to hydraulic conductivity, and describes how effectively the reservoir fluid is being transmitted for a given pressure difference, ΔP. R has been previously described as "average specific inverse mobility" [7]. S is used to calculate the reservoir parameters for the range of reservoir permeabilities considered here.

To calculate a given value of S, we determine the difference between injection and production pressure in the reservoir from TOUGH2 simulation results for six mass flowrates and eleven permeabilities, ranging from 1×10^{-15} m^2 to 1×10^{-11} m^2, at the specified depth and temperature gradient. The pressure drop, ΔP, for these 66 mass flowrate and permeability combinations is multiplied by the permeability. We then perform a linear regression of the form $\Delta P\kappa = \alpha + \beta \cdot \dot{m}$, where the intercept, α, is set to zero. The resulting slope, β, is S for that combination of depth and temperature gradient. Calculated values of S, each represented by a single data point, are shown in Fig. 2. The uncertainty in S is, on average, less than 1%, indicating the excellent characterization of the TOUGH2 numerical model, given in particular the standard assumed simulator uncertainty of ±6% (see Section S1, Supplemental information).

Fig. 2 shows that the value of $S \approx 1.14 \times 10^{-12}$ m s^{-1} for CO_2 is nearly constant over the investigated depth and geothermal gradient ranges, whereas S for brine, S_{brine}, decreases with increasing depth and temperature gradient. These values for CO_2 are likely to decrease as heterogeneities are introduced into the reservoir model [46], and S may, therefore, overestimate the pressure loss that is likely to occur. At 1 km depth and temperature gradients of 20 °C km^{-1} and 50 °C km^{-1}, S_{brine} is respectively 12 and 8 times greater than that of CO_2, which is consistent with Pruess [6]. At 5 km depth, S_{brine} decreases to 5 and 2 times greater than that of CO_2 for 20 °C km^{-1} and 50 °C km^{-1}, respectively.

For a given reservoir depth and temperature, differences in average specific kinematic viscosity, S, are due only to changes in kinematic viscosity, μ/ρ. Kinematic viscosity describes the tendency of a fluid to resist flow due to diffusion of momentum. Consequently, high kinematic viscosities result in high reservoir pressure losses and ultimately large pumping power requirements or low thermosiphon-generated mass flowrates [7]. The ratio of the kinematic viscosities of brine and CO_2 decreases with increasing depth and temperature gradient, indicating CO_2 will have comparatively lower reservoir pressure losses and pumping power requirements in shallow, cooler reservoirs.

2.3. Well and surface power plant models

Six surface power plant models and primary working fluid combinations are considered (Table 1): two direct CO_2 systems, two indirect CO_2 systems, and two indirect brine systems. The indirect systems use either R245fa or CO_2 as the secondary system working fluid. The direct CO_2 system is modeled in two ways. The "thermosiphon" system has no pumps because the flow is generated entirely by the density difference between injection and production wells [7]. The "pumped" system uses an injection pump at the surface to augment the thermosiphon flow. Surface pumps are easily maintained and less prone to failure compared to

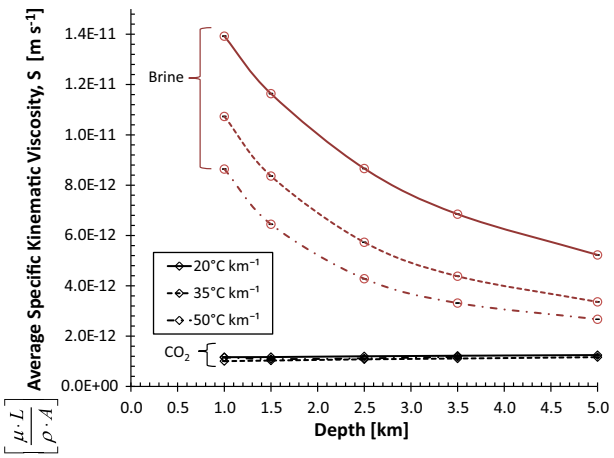

Fig. 2. Average specific kinematic viscosity, S, of a reservoir at temperatures and depths encountered for brine and CO_2 reservoir fluids.

submersible pumps. The indirect brine system, using R245fa, is the standard for current geothermal technology and requires substantial pumping by a pump submersed in the production well.

In all models, the fluid flow in the wells and surface plant are modeled using Engineering Equation Solver (EES). Brine property values are determined from the relationships provided by Driesner [47] and the IAPS-84 Steam Tables [48]. The net power, P_{net}, is the power supplied by the plant, defined in Eq. (2) as the gross turbine power plus the (negative) parasitic powers of the pumps and heat rejection equipment.

$$P_{\text{net}} = P_{\text{turbine}} + P_{\text{pump,primary}} + P_{\text{pump,ORC}} + P_{\text{fan,cooler}} + P_{\text{fan,condenser}} \quad (2)$$

2.3.1. CO_2 direct (thermosiphon and pumped)

Fluid flow through the wells and the surface power plant is illustrated in Fig. 3. Sub-cooled liquid CO_2 is injected at the surface at State 1, where it travels adiabatically and nearly isentropically down the injection well to State 2, transitioning to a supercritical fluid as pressures and temperatures increase above the critical point (T_c = 304 K, P_c = 7.4 MPa). The CO_2 then flows through the reservoir, heating to the reservoir temperature, reducing in pressure until it reaches the production well at State 3, where it is at the reservoir hydrostatic pressure. The fluid rises adiabatically [49] through the production well to State 4. Once at the surface, it is expanded through a two-phase turbine, with an assumed isentropic efficiency of 78%, based on estimated performance data from a turbine manufacturer. The fluid is then cooled and condensed isobarically through the cooling and condensing towers at the surface to State 6, where its "approach temperature" is 7 °C; that is, the fluid is cooled to 7 °C above ambient temperature. Section S4.2 of the Supplemental information discusses how this approach temperature is chosen. States 7 and 1 are determined differently for CO_2 Direct Pumped and CO_2 Direct Thermosiphon type systems.

In a CO_2 Direct Pumped system, a pump may be used to supplement the thermosiphon, and the condensation pressure (State 7) is set to 50 kPa above the saturation pressure of CO_2 at 22 °C. In this direct configuration, either a pump or throttle valve is used between States 7 and 1 (Fig. 3) to achieve the greatest net power. The net power tends to increase with some pumping, but there are some scenarios in which a decrease in pressure between States 7 and 1 reduces the overall system mass flowrate. This reduction in mass flowrate decreases the condenser parasitic power losses more than the decrease in turbine power and thus increases net power output. As a consequence, throttling by a valve is used in approximately 10% of the Direct CO_2 Pumped scenarios, typically where the turbine is operated near the critical point of CO_2. In this fraction of scenarios, the power outputs of the Direct CO_2 Pumped and Thermosiphon systems are the same.

In a CO_2 Direct Thermosiphon system, the condensation pressure (State 7) is set to achieve a pressure at State 2, which is equivalent to the sum of the hydrostatic reservoir pressure and the reservoir pressure change; however, the pressure at State 7 may never be less than 50 kPa above the saturation pressure of CO_2 at 22 °C. In some CO_2 Direct Thermosiphon systems, a throttle valve is added between State 7 (after the condenser) and State 1 (injection well) to decrease the system mass flowrate. Such throttling decreases the pressure losses in the production well and the reservoir, increasing the temperature at State 4, decreasing the fluid density in the turbine, and thus increasing the power generated by the turbine.

The fluid state in the injection and production wells is calculated numerically with 100 m long axial elements. This element size is chosen to balance computational time with the precision of the results; results for 100 m long elements are within 1% of

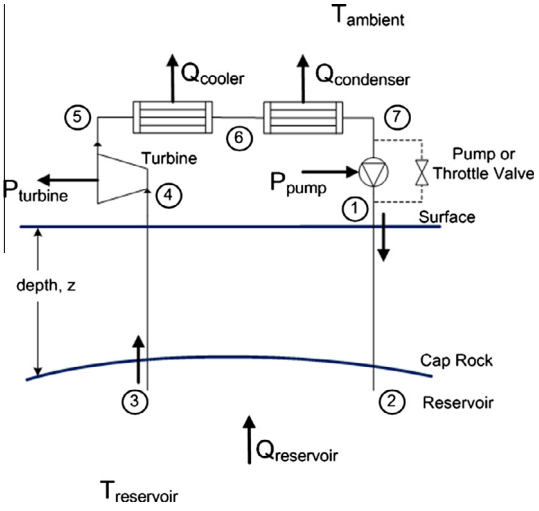

Fig. 3. Direct CO_2 System.

results for a finely discretized model using 1 m segments. Across each vertical well element, the first law of thermodynamics, patched Bernoulli, and the conservation of mass equations are used to determine the state of each successive starting element, as shown in Eqs. (3)–(6), where subscripts i and $i+1$ denote the beginning and end of each element, respectively. All nomenclature is described in Table 3. The well segments are considered to be adiabatic [49], but not isenthalpic as assumed in earlier studies [50,6].

$$h_i + \frac{V_i^2}{2} + gz_i = h_{i+1} + \frac{V_{i+1}^2}{2} + gz_{i+1} \quad (3)$$

$$P_i + \frac{\rho_i V_i^2}{2} + \rho_i g z_i = P_{i+1} + \frac{\rho_i V_{i+1}^2}{2} + \rho_i g z_{i+1} - \Delta P_{\text{loss}} \quad (4)$$

$$\Delta P_{\text{loss}} = f \frac{L_{\text{pipe}}}{D} \frac{\rho V^2}{2} = f \frac{L_{\text{pipe}}}{D^5} \frac{8\dot{m}^2}{\rho \pi^2} \quad (5)$$

$$\dot{m} = \rho_i A V_i = \rho_{i+1} A V_{i+1} \quad (6)$$

The friction factor, f, is determined using the Moody Chart, based on the pipe inner diameter, surface roughness, and Reynolds number [51]. A pipe surface roughness of 55 μm is used to approximate bare CR13 piping, a standard oil and gas martensitic stainless steel piping used in corrosive environments, as suggested by

Table 3
Nomenclature.

A	A Effective vertical cross-section of reservoir (m^2)
D	Well pipe diameter (m)
f	Darcy friction factor (–)
g	Gravitational constant (9.81 m s^{-2})
h	Specific enthalpy (kJ kg^{-1})
L	Effective reservoir length (m)
L_{pipe}	Pipe length (m)
$\dot{m}$	Fluid mass flowrate (kg s^{-1})
P	Pressure (kPa)
P_{net}	Net power generated (kW_e)
Q	Heat energy transfer rate (kW_{th})
R	Reservoir parameter (kPa s kg^{-1})
S	Average specific kinematic viscosity (m s^{-1})
T	Temperature (°C)
V	Velocity (m s^{-1})
z	Elevation (m)
κ	Scalar reservoir permeability (m^2)
μ	Dynamic fluid viscosity (N s m^{-2})
ρ	Fluid density (kg m^{-3})

Farshad and Rieke [66]. This value overestimates pressure losses when compared with the typical 45 μm value suggested by Moody [51] for schedule 40 pipe.

Additionally, pressure losses (ΔP_{loss} in Eq. (5)) are proportional to the square of the mass flowrate, $\dot{m}$, and inversely proportional to the fifth power of the pipe diameter, D. Hence, power production is sensitive to small changes in D. Furthermore, for the same mass flowrate, pressure losses decrease as fluid density increases; therefore, pressure losses in the injection well, where fluids are relatively cool and thus dense, are usually a small fraction of those in the production well, where fluids are relatively hot and thus less dense.

$$Q - P = \dot{m}(h_{out} - h_{in}) \tag{7}$$

The power and heat values are found from the enthalpy difference of the fluid, shown in Eq. (7). Specifically, the power output of the turbine is the product of the difference of inlet and exit enthalpies, found using the isentropic turbine efficiency and the mass flowrate. Similarly, the pump power is found using the isentropic pump efficiency. The heat extraction rates for the reservoir, cooling, and condensing towers are the products of the enthalpy difference, between inlet and outlet, and the mass flowrate (Eq. (7)). The parasitic power requirements of the cooling and condensing towers are the product of the heat extraction rate and the parasitic loss fraction, λ, which is described in Section S2 of the Supplemental information. The net power varies as a function of mass flowrate, as shown in Fig. 4, for the base-case Direct CO_2 Thermosiphon (un-pumped) system. As mass flowrate increases, the power gains provided by increased turbine throughput are offset by the pressure losses incurred in the piping and reservoir, yielding a point of optimum power. Thus, the mass flowrate through the system is chosen to maximize the net power produced and is further described in Section S4.1 of the Supplemental information.

2.3.2. Indirect CO_2 and brine

In an indirect system, the primary, i.e., subsurface geothermal, working fluid passes through a heat exchanger, driving a secondary Rankine cycle, as shown in Fig. 5. Indirect systems benefit from using "off-the-shelf" components and have fewer moving parts in contact with the geothermal fluid, but they have smaller overall system thermal efficiency. The Rankine cycle consists of six major components: a preheater (States 13 to 14), a boiler (States 14 to 9), a turbine (States 9 to 10), a de-superheater (States 10 to 11), a condenser (States 11 to 12), and a pump (States 12 to 13). Advanced Rankine technology (e.g., multi-stage turbines and regenerators) are beyond the scope of this paper, but they may increase cycle efficiency with some working fluids [52,53]. Superheating is

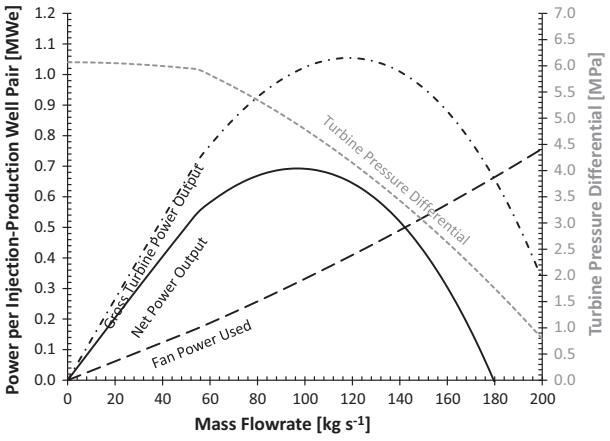

Fig. 4. Power output of a direct CO_2 thermosiphon (un-pumped) system for one injection–production well pair (base-case) of which 4 such pairs constitute one 5-spot system.

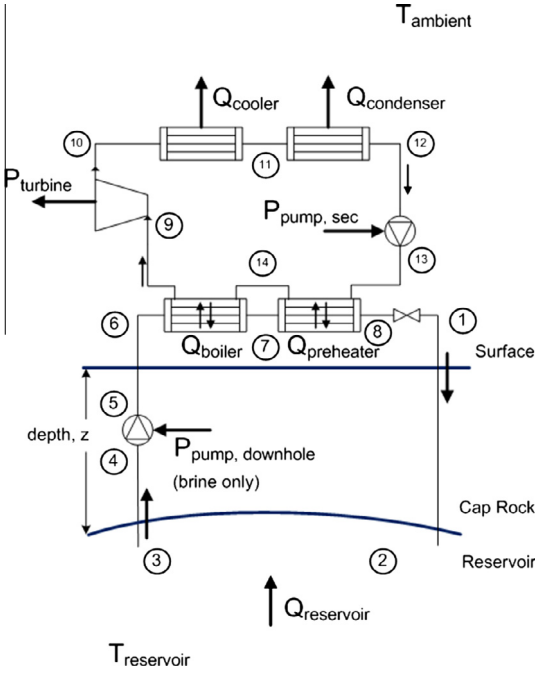

Fig. 5. Indirect brine or CO_2 geothermal system.

applied when it is necessary to set the turbine outlet or the pump inlet at a saturated state, depending on the saturation curve characteristics of the secondary working fluid. The CO_2 and brine subsurface working fluid systems are modeled almost identically, except the brine system requires a downhole pump (States 4 to 5). The wells (States 1 to 2, 3 to 4 and 5 to 6) are modeled the same way as in the direct CO_2 system, using their respective brine or CO_2 fluid property values. Turbomachinery efficiencies are listed in Table 2 and are typical of ORC simulations [65].

At the surface, in the primary working fluid loop, the fluid passes isobarically through a boiler (R245fa only) and a preheater, arriving at State 8. Then the fluid flows isenthalpically through a throttling valve, used to reduce the pressure and control the mass flowrate (CO_2 only), where it arrives at State 1 and is reinjected through a well into the reservoir. No geothermal pumps are used in the indirect geologic-CO_2 system because the energy they require is greater than the increase in power they produce. Unlike the direct system, the indirect system does not drive a pressure reduction device (e.g., turbine) at the surface; therefore, the indirect geologic-CO_2 system operates at higher primary-fluid mass flowrates than its direct counterpart, and is driven by the additional pressure potential otherwise used to operate the turbine.

The secondary cycle is a trans-critical (CO_2) or sub-critical (R245fa) Rankine cycle. Low density fluid leaves the boiler at State 9 and is expanded through the turbine to either a superheated vapor (R245fa) or a saturated vapor (CO_2) at State 10. The fluid is then cooled isobarically to saturation at State 11 (R245fa only), and then condensed isobarically to State 12 at a saturation pressure that is 7 °C above ambient temperature (7 °C approach temperature). The high density liquid is then pumped to a high pressure sub-cooled liquid at State 13. When using R245fa, it is heated to boiling at State 14, and then heated to a saturated vapor at State 9. In the case of the trans-critical CO_2 Rankine cycle, the supercritical fluid is heated from State 13 to State 9, increasing in temperature throughout with no discernible phase change.

When R245fa is used as the secondary working fluid, the temperature of the primary fluid within the heat exchanger is set to be at least 7 °C hotter than the R245fa secondary fluid at any location; this value was obtained as a compromise between cost and

performance in unreported optimization simulations. This restriction specifies that the fluid temperature at State 7 must be at least 7 °C above the boiling temperature of the R245fa, and the temperature at State 8 must be at least 7 °C above the condensing temperature of the R245fa. These 7 °C specifications can result in a "pinch point" problem, where the fluid outlet temperature at State 8 is much higher than 7 °C above ambient and the injected fluid contains useful thermal energy. Injecting unused energy results in decreased cycle efficiency, decreased density in the injection well, and diminished mass flowrate produced by the thermosiphon effect. Conversely, injecting unused energy into the reservoir does extend the reservoir lifespan. Low-temperature solar energy can be used to assist with boiling the secondary working fluid, to decrease injection temperature and mitigate the pinch-point problem [54], but, we did not use this method here.

When CO_2 is used as the secondary working fluid, the heat exchanger pinch point problem is alleviated. The CO_2 on the high-pressure side of the Rankine Cycle is a supercritical fluid and does not boil; it has a nearly constant temperature gradient, which matches the decreasing temperature profile of the primary working fluid passing through the counter-flow heat exchanger. For these CO_2 simulations, the boiler is removed so that all heat transfer occurs within the preheater.

When using R245fa or CO_2 as the secondary fluid, the plant operator selects either the secondary boiling temperature (R245fa) or the secondary high-side pressure (CO_2), which yields the largest net power. We determine the operating points for these indirect systems (see Section S3 of the Supplemental information).

In contrast to the indirect CO_2-geology-based systems that increase the mass flowrate, and thus power, most effectively by cooling the injected fluid, the indirect brine-geology-based systems produce increased net power when pumped [55]. Therefore, a downhole lineshaft pump is placed 500 m down the production well (States 4 to 5 in Fig. 5) in all subsurface brine scenarios. The pumping power is allowed to vary in order to attain the maximum net power output of the system. A maximum pumping pressure difference of 10 MPa is set, based on the limit of currently available geothermal downhole lineshaft Vertical Industrial Turbine pumps available from Goulds [56], which is approximately 3 times larger than what was allowed by Sanyal and Butler [38].

When using a brine system, flashing can occur at the surface if piping pressure losses decrease the brine pressure below its saturation pressure; therefore, the minimum pressure in the system is maintained above the condensing pressure for the brine. To allow this flexibility, the downhole well pressure is always above or below the hydrostatic pressure of the reservoir. This overpressurization is generally small: 1400 kPa on average and a standard deviation of 2020 kPa above hydrostatic pressure for the parameter space investigated. Minimum and maximum under/overpressurizations are −2440 kPa and 10,440 kPa, respectively. Therefore, the calculated mass flowrate values for the brine are a high limit and will decrease based on the actual reservoir pressure.

The injection temperature of the brine is limited by the saturation temperature of dissolved amorphous silica. In the reservoir, the brine is saturated with dissolved quartz. When the brine is produced to the surface and cools more than 122 °C (89 °C) for 0 wt% NaCl brine (20 wt% NaCl brine), the quartz precipitates from the solution as amorphous silica [57]. This causes scaling within the piping and turbomachinery and is avoided by maintaining the brine above the saturation temperature of amorphous silica.

3. Parameter space results

Six surface plant models, six reservoir permeabilities, five depths, three geothermal temperature gradients, and four well diameters have been investigated (Table 1), resulting in 5670 individual electric power production values. For comparison, a subset of these values is shown in Fig. 6 providing 225 values each for the direct CO_2 (with pumping) system and the indirect brine system (which is always pumped) with R245fa as the secondary working fluid. The indirect brine/R245fa case most closely represents the current state of technology for geothermal power production as none of the other systems are commercially available. Tables for all six surface plants can be found in Section S5 of the Supplemental information. All power production and mass flowrate data are available in Section S6 of the Supplemental information.

Power output from both systems increases with increases in: reservoir depth and permeability, thermal gradient, and well diameter. The values in Fig. 6 correspond to a single injection–production well pair and must be multiplied by four to obtain the total power output of a complete inverted 5-spot well system (Fig. 1). Injection–production well pair electric power output values in Fig. 6 are color-coded, indicating low (red)[1], moderate (yellow), or substantial (green) power production rates. The base case is bounded by the two boxed values, producing approximately 0.7 MWe (2.8 MWe total for the inverted 5-spot well pattern) at a depth of 2.5 km, increasing more than five times to 3.7 MWe (14.8 MWe) when the depth increases to 5.0 km.

In contrast, power output at a depth of 1.0 km is negligible for all cases. Similarly, for a 20 °C km^{-1} thermal gradient with reservoir depths 2.5 km and shallower, and for a 35 °C km^{-1} geothermal gradient with reservoir depths 1.5 km and shallower, negligible amounts of power are produced.

Fig. 7 shows the difference in electric power generation for the two systems represented by Fig. 6, i.e., between a direct, pumped CO_2 system and a pumped indirect brine system with the latter employing an R245fa secondary power loop. Positive numbers indicate parameters where the CO_2 system produces more power than the brine system.

Direct CO_2 systems produce more power than brine systems, which are always indirect, in shallower and less permeable reservoirs. The few instances where brine systems produce more power are in hot, particularly permeable locations. The difference between the two systems is most pronounced at a permeability of 5×10^{-14} m^2, due to the lower pressure losses of CO_2, relative to those of brine, as it flows through the reservoir (Fig. 2). At high permeability, the reservoir pressure losses of each system are negligible and the brine systems can produce more power because of the larger heat capacity of brine. Consequently, the direct CO_2 system behaves quite differently than its brine alternative, and will produce more power in shallower, cooler, less permeable environments.

Of particular interest is the substantially larger power production in the 50 °C km^{-1}, 5.0 km scenarios of the direct CO_2 system. While CO_2 tends to produce more power in shallower, cooler, less permeable cases, in agreement with Carroll and Stillman [21]; it deviates from their findings by also producing more power in very hot and deep environments, where the injection temperature of the brine is limited to prevent silica precipitation [57] as shown in Fig. 7. As CO_2 is a relatively poor solvent of minerals, it has no such limitation and is able to extract more thermal energy from the geologic fluid, producing more power than brine.

3.1. Comparison of net electric power output for the six systems for the base case

The six systems are compared using the base-case parameters and depths from 1 to 5 km. The results provided in Fig. 8 show that

[1] For interpretation of color in 'Fig. 6', the reader is referred to the web version of this article.

(a)

Direct CO_2 - Pumped

Power Output per Production-Injection Pair [MWe]

Temp Gradient [°C km^{-1}]	Depth [km]	0.27m Inj & Prod Diameter					0.33m Inj & Prod Diameter					0.41m Inj & Prod Diameter				
		1x10^{-15} m^2	1x10^{-14} m^2	5x10^{-14} m^2	1x10^{-13} m^2	1x10^{-12} m^2	1x10^{-15} m^2	1x10^{-14} m^2	5x10^{-14} m^2	1x10^{-13} m^2	1x10^{-12} m^2	1x10^{-15} m^2	1x10^{-14} m^2	5x10^{-14} m^2	1x10^{-13} m^2	1x10^{-12} m^2
20	1.0	0.0	0.0	0.0	0.0	0.0	0.0	0.0	0.0	0.0	0.0	0.0	0.0	0.0	0.0	0.0
	1.5	0.0	0.0	0.0	0.0	0.0	0.0	0.0	0.0	0.0	0.0	0.0	0.0	0.0	0.0	0.0
	2.5	0.0	0.0	0.0	0.0	0.0	0.0	0.0	0.0	0.1	0.1	0.0	0.0	0.0	0.1	0.1
	3.5	0.0	0.0	0.1	0.1	0.1	0.0	0.0	0.1	0.2	0.2	0.0	0.0	0.2	0.3	0.4
	5.0	0.0	0.1	0.3	0.3	0.4	0.0	0.2	0.4	0.5	0.6	0.0	0.2	0.6	0.8	1.1
35	1.0	0.0	0.0	0.0	0.0	0.0	0.0	0.0	0.0	0.0	0.0	0.0	0.0	0.0	0.0	0.0
	1.5	0.0	0.0	0.1	0.1	0.1	0.0	0.0	0.1	0.2	0.2	0.0	0.0	0.2	0.3	0.3
	2.5	0.0	0.2	0.5	0.6	0.6	0.0	0.2	0.7	0.9	1.1	0.0	0.3	0.9	1.3	1.8
	3.5	0.1	0.6	1.0	1.1	1.2	0.1	0.7	1.6	1.8	2.1	0.1	0.7	2.3	2.9	3.6
	5.0	0.2	1.5	2.3	2.5	2.6	0.2	1.9	3.7	4.0	4.4	0.2	2.2	5.6	6.5	7.7
50	1.0	0.0	0.0	0.0	0.0	0.0	0.0	0.0	0.1	0.1	0.1	0.0	0.0	0.1	0.1	0.1
	1.5	0.0	0.2	0.6	0.7	0.7	0.0	0.3	0.8	1.0	1.2	0.0	0.3	1.1	1.5	2.1
	2.5	0.1	0.8	1.6	1.7	1.9	0.1	1.0	2.4	2.7	3.1	0.1	1.0	3.4	4.3	5.4
	3.5	0.3	1.9	3.0	3.2	3.4	0.3	2.3	4.7	5.2	5.7	0.3	2.6	7.0	8.4	10.0
	5.0	0.8	4.4	6.0	6.2	6.5	0.8	5.9	9.6	10.2	10.9	0.8	7.2	15.3	17.1	19.1

(b)

Indirect Brine (R245fa) - Pumped

Power Output per Production-Injection Pair [MWe]

Temp Gradient [°C km^{-1}]	Depth [km]	0.27m Inj & Prod Diameter					0.33m Inj & Prod Diameter					0.41m Inj & Prod Diameter				
		1x10^{-15} m^2	1x10^{-14} m^2	5x10^{-14} m^2	1x10^{-13} m^2	1x10^{-12} m^2	1x10^{-15} m^2	1x10^{-14} m^2	5x10^{-14} m^2	1x10^{-13} m^2	1x10^{-12} m^2	1x10^{-15} m^2	1x10^{-14} m^2	5x10^{-14} m^2	1x10^{-13} m^2	1x10^{-12} m^2
20	1.0	0.0	0.0	0.0	0.0	0.0	0.0	0.0	0.0	0.0	0.0	0.0	0.0	0.0	0.0	0.0
	1.5	0.0	0.0	0.0	0.0	0.0	0.0	0.0	0.0	0.0	0.0	0.0	0.0	0.0	0.0	0.0
	2.5	0.0	0.0	0.0	0.0	0.0	0.0	0.0	0.0	0.0	0.0	0.0	0.0	0.0	0.0	0.0
	3.5	0.0	0.0	0.0	0.1	0.2	0.0	0.0	0.0	0.1	0.3	0.0	0.0	0.0	0.1	0.4
	5.0	0.0	0.1	0.4	0.5	0.8	0.0	0.1	0.4	0.7	1.3	0.0	0.1	0.4	0.8	2.1
35	1.0	0.0	0.0	0.0	0.0	0.0	0.0	0.0	0.0	0.0	0.0	0.0	0.0	0.0	0.0	0.0
	1.5	0.0	0.0	0.0	0.0	0.0	0.0	0.0	0.0	0.0	0.1	0.0	0.0	0.0	0.0	0.1
	2.5	0.0	0.0	0.2	0.3	0.6	0.0	0.0	0.2	0.4	0.9	0.0	0.0	0.2	0.4	1.5
	3.5	0.0	0.3	1.1	1.5	2.1	0.0	0.3	1.4	2.1	3.5	0.0	0.3	1.5	2.6	5.9
	5.0	0.1	1.1	3.2	3.8	4.5	0.1	1.2	4.2	5.6	7.6	0.1	1.2	5.1	7.9	13.0
50	1.0	0.0	0.0	0.0	0.0	0.0	0.0	0.0	0.0	0.0	0.0	0.0	0.0	0.0	0.0	0.1
	1.5	0.0	0.0	0.1	0.1	0.4	0.0	0.0	0.1	0.1	0.6	0.0	0.0	0.1	0.1	0.8
	2.5	0.0	0.4	1.4	1.9	2.7	0.0	0.4	1.6	2.5	4.4	0.0	0.4	1.7	3.1	7.4
	3.5	0.1	1.1	3.5	4.4	5.4	0.1	1.2	4.5	6.3	8.9	0.1	1.2	5.3	8.6	15.3
	5.0	0.1	1.5	3.5	4.1	4.6	0.1	1.5	4.9	6.2	7.7	0.1	1.6	6.3	9.1	13.3

Fig. 6. Net electric power production (in MWe) per injection–production well pair for (a) direct CO_2-pumped and (b) indirect (binary) brine-pumped (R245fa) systems.

for a given permeability, temperature gradient, and well diameter, all six systems produce more net electric power as the depth, therefore the reservoir temperature, and therefore system thermodynamic efficiency, increase. Pumped and thermosiphon direct CO_2 systems provide greater net power than the brine options until a depth of approximately 3.5 km. The pumped CO_2 system always produces more net power than its thermosiphon-driven, unpumped counterpart. Direct CO_2 systems produce more net power than indirect CO_2 systems except at 5 km, where the indirect CO_2 (with CO_2 as secondary working fluid) system produces 0.2 MWe (5%) more net power than the Direct CO_2 Thermosiphon system.

Using CO_2 as the secondary Rankine cycle working fluid generally produces more net power than when using R245fa. For example, the use of CO_2 as a secondary working fluid, on average, increases net power production by 22% and 20% for brine and CO_2 systems, respectively. CO_2 Rankine cycles are trans-critical and do not have the "pinch point" problem during heating, as discussed before, and can thus extract more energy from the primary geologic fluid than systems that employ R245fa as the secondary working fluid. This result is consistent with Maraver et al. [58]. Systems that have a temperature glide (i.e. non-constant temperature heat addition) will tend to avoid the "pinch point" problem and have higher utilization efficiencies [53]. Future work might include the addition of R32 into the secondary CO_2 working fluid, which creates a zeotropic mixture that shifts the ORC to a Brayton cycle, increasing overall heat rejection temperatures, reducing parasitic losses, and decreasing overall cycle pressure [59].

In rare circumstances, such as the 5.0 km, 35 °C km^{-1} brine scenario shown in Fig. 8, systems with R245fa as the secondary working fluid produce more net power than trans-critical CO_2 systems

Temp Gradient [°C km^{-1}]	Depth [km]	0.27m Inj & Prod Diameter					0.33m Inj & Prod Diameter					0.41m Inj & Prod Diameter				
		1x10^{-15} m^2	1x10^{-14} m^2	5x10^{-14} m^2	1x10^{-13} m^2	1x10^{-12} m^2	1x10^{-15} m^2	1x10^{-14} m^2	5x10^{-14} m^2	1x10^{-13} m^2	1x10^{-12} m^2	1x10^{-15} m^2	1x10^{-14} m^2	5x10^{-14} m^2	1x10^{-13} m^2	1x10^{-12} m^2
20	1.0															
	1.5															
	2.5														0.1	0.1
	3.5			0.1					0.1	0.1				0.1	0.2	
	5.0			-0.1	-0.2	-0.4		0.1		-0.2	-0.6		0.1	0.1		-1.0
35	1.0															
	1.5			0.1	0.1	0.1			0.1	0.2	0.1			0.2	0.3	0.2
	2.5		0.2	0.3	0.3			0.2	0.5	0.5	0.1		0.2	0.7	0.9	0.3
	3.5	0.1	0.3	-0.1	-0.4	-0.9	0.1	0.3	0.2	-0.3	-1.4		0.4	0.8	0.2	-2.3
	5.0	0.1	0.4	-0.8	-1.3	-1.9	0.1	0.8	-0.6	-1.6	-3.2	0.1	1.0	0.5	-1.3	-5.4
50	1.0								0.1	0.1				0.1	0.1	0.1
	1.5		0.2	0.5	0.5	0.4		0.2	0.7	0.9	0.7		0.2	1.0	1.3	1.3
	2.5	0.1	0.5	0.2	-0.2	-0.8	0.1	0.6	0.8	0.2	-1.3	0.1	0.7	1.7	1.2	-1.9
	3.5	0.2	0.8	-0.5	-1.1	-2.0	0.2	1.2	0.2	-1.1	-3.2	0.2	1.5	1.7	-0.2	-5.3
	5.0	0.7	3.0	2.5	2.2	1.9	0.7	4.3	4.7	4.0	3.2	0.7	5.6	9.0	7.9	5.8

Fig. 7. Electric power production difference per injection–production well pair between the direct pumped CO_2 and the indirect (binary) brine (R245fa) systems in MWe.

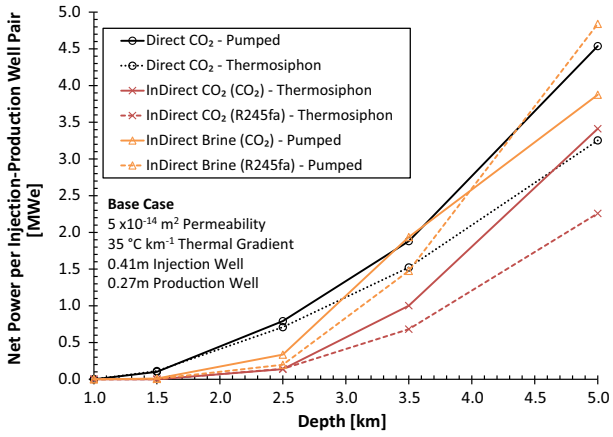

Fig. 8. Net power output comparison of all six power systems (base-case).

due to boiler and preheater temperatures that allow a majority of the heat to be extracted from the primary, i.e., subsurface, geologic working fluid. The net power output of the brine system is further limited in the 5.0 km case by the 101 °C injection temperature limitation to prevent the precipitation of amorphous silica, as discussed previously.

When CO_2 is the primary subsurface heat extraction fluid, a Rankine cycle with CO_2 as the secondary working fluid always produces more net power than using R245fa as the secondary working fluid. This results from employing matched primary and secondary working fluids within the counter-flow heat exchanger, which allows a majority of the heat to be transferred with few thermodynamic losses.

3.2. Electric power breakdown for the base case

Rankine cycles using CO_2 as the secondary working fluid are able to extract more heat from the geothermal fluid than those that use R245fa; however, R245fa cycles tend to have a higher thermal efficiency, consistent with other low-temperature ORC refrigerant comparisons [60]. The decreased thermal efficiency when employing CO_2 as the secondary working fluid is due to its large secondary-loop pumping requirement. This is shown in Fig. 9 by the allotment of power for individual system components. The total height of each bar indicates the gross turbine power output; the net power output for each scenario is shown by the blue (bottom) bar.

Direct systems have the smallest number of components and the least parasitic power losses—for the base case shown in Fig. 9, only 32% of the gross turbine power for the thermosiphon direct CO_2 system is consumed by the fan power for the cooling towers. Conversely, when CO_2 is used as the secondary working fluid in an indirect system, 78–85% of the gross turbine output can be consumed by parasitic losses. The losses drop to 60% when R245fa is used as the secondary working fluid. Despite the larger parasitic loss fractions, the net power output for the CO_2 indirect systems tends to be larger than the R245fa systems.

When CO_2 is used as the secondary working fluid, the ORC pump is a large source of parasitic losses. This is due to the small difference in density between the pump and turbine. The pressure differences across both the pump and turbine in a Rankine cycle are essentially equal, but the power is inversely proportional to the density of the fluid that passes through, $P_{\text{turbine/pump}} = \dot{m} \int \frac{1}{\rho} dP$, described in substantial detail in Adams

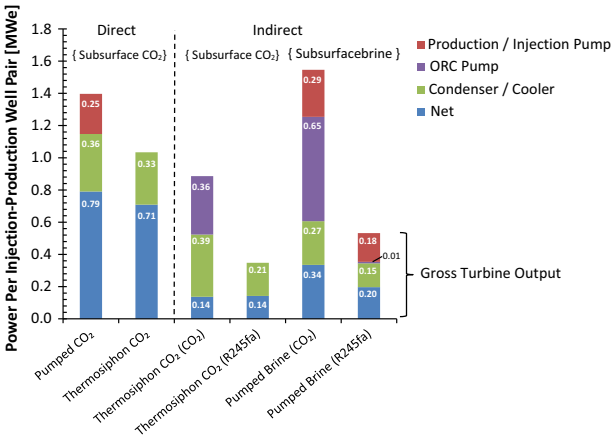

Fig. 9. Electric power per injection–production well pair (MWe) breakdown of all six power systems investigated (base case).

et al. [55]. When R245fa is used, the density difference is about two orders of magnitude, decreasing from roughly 1300 kg m^{-3} in the pump to 10 kg m^{-3} in the turbine. When CO_2 is used, the reduction in density (800 kg m^{-3} in the pump to 150 kg m^{-3} in the turbine) is much more moderate. The result is that the pumping power, when using CO_2 as the secondary working fluid, can be half the total parasitic loss, as shown in Fig. 9. However when considering the substantially higher rate of heat input obtained by a constant temperature difference between both fluids in the heat exchanger, the CO_2 system will generate more net power, typical of supercritical systems [61]. The advantage of using CO_2 as the secondary working fluid diminishes in particularly deep, hot geothermal systems, where R245fa has a similar rate of heat input, but higher thermal efficiency.

3.3. Electric power production influenced by well diameter

Electric power production depends on fluid mass flowrate, which is influenced by the pressure losses in the wells and in the reservoir [7]. Therefore, the well diameter may substantially impact the power output of a system. Four well diameters are investigated in varying combinations between the injection and production wells for the indirect brine, with R245fa as the secondary working fluid, and for the CO_2 direct base-case scenarios. The resulting net power outputs are shown in Fig. 10 as a function of the other major factor of pressure loss: reservoir permeability.

Electric power production increases as the well diameter increases, as expected. The effect of well diameter increase in power production is more pronounced for more permeable reservoirs. When a 0.14 m well diameter is used, system power output is restricted to low values—at most 0.25 MWe and 0.35 MWe for CO_2 and brine, respectively—independent of reservoir permeability, because the majority of system pressure losses occur within the wells. Likewise, at small permeabilities below 10^{-14} m^2 for CO_2 and below 10^{-13} m^2 for brine, the well diameter does not have much impact, but as the reservoir permeability increases, the diameter begins to have a larger impact on power production. Finally, at high reservoir permeabilities of $\sim 10^{-12}$ m^2, the power production curves for CO_2 tend to level off with further permeability increases. This differs from brine, for which reservoir pressure losses are still substantial at a permeability of 10^{-12} m^2, where the curves have not yet inflected; however, the occurrence of reservoir permeability larger than 10^{-12} m^2 appears unlikely [15,16].

In unreported simulations, injection and production wells are sized to equate pressure losses in each well, but it appears that no sizing guidelines have emerged from these results—except that increasing well diameter always produces more power.

3.4. Surface plant and reservoir pairing

We evaluate the six systems to determine how net power production varies with reservoir permeability, otherwise using base-case parameters. The resultant power curves are shown in Fig. 11.

Direct CO_2 systems produce more power than brine systems at permeabilities below about 2×10^{-13} m^2, while brine systems produce more power at higher permeabilities. Indirect CO_2 systems exhibit low power production throughout the range of permeabilities examined due to the constant low production temperature ($\sim$59 °C) and therefore low thermal efficiency of the Rankine cycle. Unlike brine, which drops in pressure substantially but maintains its temperature, CO_2 expands in the production well with moderate decreases in both temperature and pressure. Indirect brine Rankine systems have a higher thermal efficiency due to the higher brine production temperature ($\sim$102 °C); therefore larger amounts of power are produced when the permeability increases and the system mass flowrate correspondingly increases. Despite the low

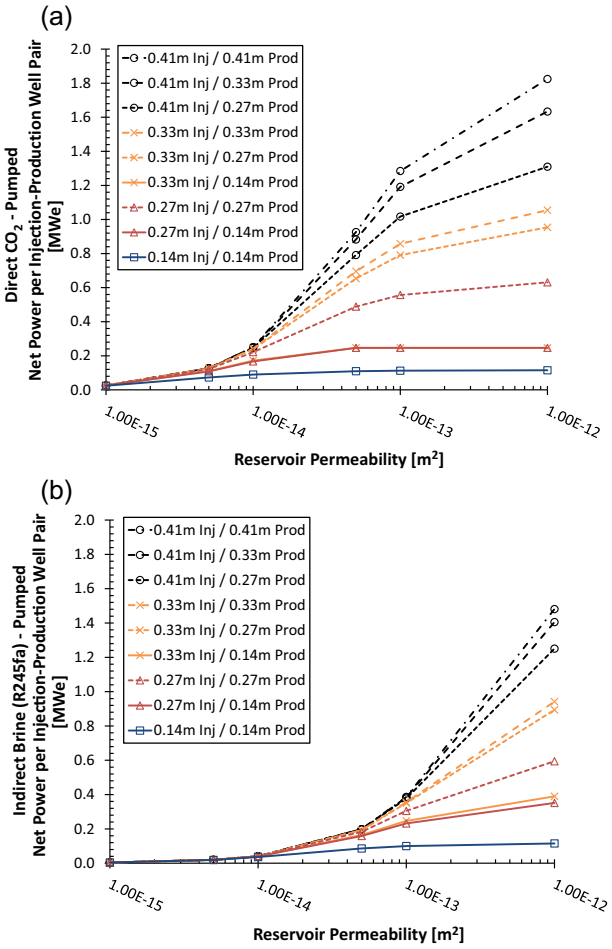

Fig. 10. Net power output dependence on well diameter and reservoir permeability for (a) direct pumped CO_2 and (b) indirect pumped brine, the latter with R245fa as the secondary working fluid (base case).

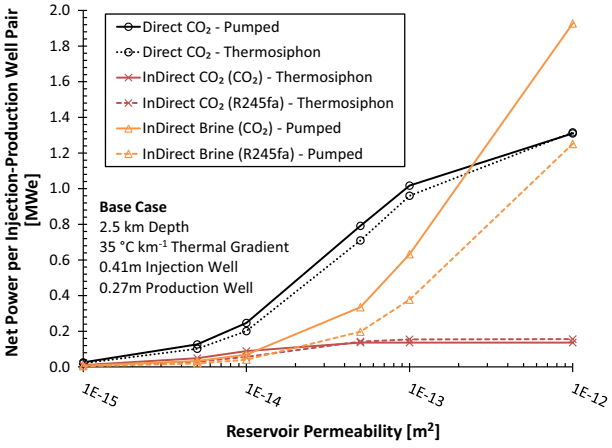

Fig. 11. Net electric power output dependence on system type and reservoir permeability (base case).

production temperature ($\sim$59 °C), direct CO_2 systems produce power by using the large pressure differential between the production and injection wellheads to drive a turbine and therefore have a comparable thermal efficiency to the overall indirect brine system.

At the base-case permeability of 5×10^{-14} m^2, the direct CO_2 pumped system produces more power than brine by a factor of 2.3 and 4.1, for CO_2 and R245fa secondary systems, respectively. The decreasing slope of the CO_2 curves at high permeabilities,

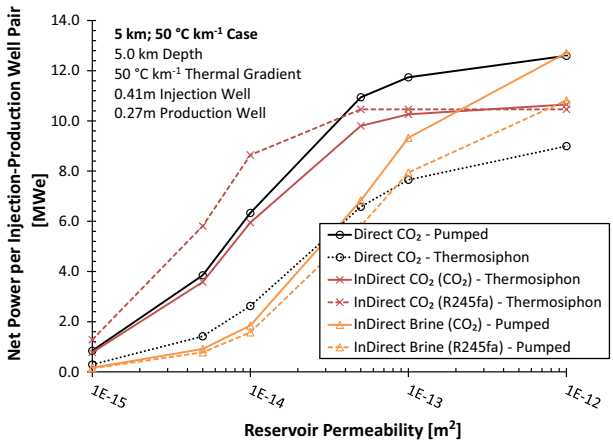

Fig. 12. Net electric power output dependence on system type and reservoir permeability (5 km; 50 °C km^{-1}).

shown in Fig. 11, indicates that the reservoir pressure losses are becoming less significant and are thus no longer the limiting factor in power production. However the reservoir pressure losses, when using brine, continue to be a significant fraction of the overall system pressure losses. Thus increases in reservoir permeability continue to increase power production for the brine systems. Even at high permeabilities (1×10^{-12} m^2), the reservoir parameter (Eq. (1)) for brine is R = 5.7 kPa s kg^{-1}, compared to R = 1.1 kPa s kg^{-1} for CO_2, resulting in greater pressure losses by a factor of 5.3 in the reservoir when using brine than when using CO_2. Overall, the results suggest that, at minimum, direct CO_2 systems exhibit beneficial electric power production characteristics for permeabilities less than 10^{-13} m^2, compared to traditional brine systems.

Net electric power production for most of the combinations of depth and thermal gradient follow a similar trend to those listed above for the base case; however, at a depth of 5 km and a geothermal gradient of 50 °C km^{-1}, as shown in Fig. 12, several of the trends reverse: the indirect CO_2 (R245fa) system can produce more net power than the direct pumped CO_2 system; the brine systems never have a larger net power production than the direct pumped CO_2 system; and the indirect CO_2 system has larger net power production when using R245fa, instead of CO_2, as the secondary working fluid.

At a depth of 5 km and a geothermal gradient of 50 °C km^{-1}, the advantage of using CO_2 as the reservoir heat extraction fluid is at its weakest of the investigated cases as S_{brine} is only larger than S_{CO2} by a factor of 2.2 (Fig. 2). Despite the comparable pressure losses of brine at these depths and pressures, the brine systems do not produce more net power than CO_2. This is largely due to the Silica precipitation constraint which limits the temperature reduction of the produced brine to only 85 °C, necessitating the re-injection of 174 °C brine into the reservoir, which still contains useful thermal energy. The CO_2-based systems do not suffer from this constraint.

In addition, at this high reservoir temperature, the indirect CO_2 (R245fa) system produces more power than the direct pumped CO_2 system at permeabilities less than 5×10^{-14} m^2. At a permeability of 10^{-14} m^2, the indirect CO_2 (R245fa) system has a mass flowrate of 182 kg s^{-1}, compared to 160 kg s^{-1} for indirect CO_2 (CO_2), 167 kg s^{-1} for direct pumped CO_2, and 48 kg s^{-1} for indirect brine (R245fa) systems. The high mass flowrate of the indirect CO_2 (R245fa) system, combined with its high ORC thermal efficiency, low pumping loads, and a minimal pinch-point constraint cause this system to produce more power under these reservoir conditions than the CO_2 (CO_2) system, which is uncommon.

4. Conclusions

We modeled comparable CO_2 and brine geothermal systems in sedimentary basins. We provide the following conclusions:

CO_2 experiences less pressure loss in a sedimentary reservoir than brine at comparable fluid mass flowrates. The pressure loss through a reservoir is directly proportional to the fluid's average specific kinematic viscosity, S, for a given reservoir permeability. At a 1 km depth, S for brine, S_{brine}, is 8–12 times greater than S for CO_2, denoted S_{CO2}. At 5 km, S_{brine} decreases to 2 to 5 times greater than S_{CO2}. The ratio S_{brine}/S_{CO2} decreases with increasing depth and temperature, indicating CO_2 has significantly lower reservoir pressure losses and pumping power requirements in relatively shallower, cooler reservoirs, compared to brine.

CO_2 direct systems produce more net power than brine systems at low to moderate reservoir depths and permeabilities. CO_2 direct systems produce net power at depths as shallow as 1.5 km, and consistently more net power than brine systems until depths of about 3.5 km. Additionally, at permeabilities below 10^{-13} m^2, CO_2 can produce much more power than brine. For example, in the base-case scenario, at a permeability of 5×10^{-14} m^2 and a depth of 2.5 km, the direct pumped CO_2 system produces a factor of 4.1 times more net power than the indirect brine system with R245fa as the secondary Rankine fluid (current state-of-the-art technology). The comparative advantage for using CO_2 is a result, in part, of the generally low average specific kinematic viscosity, S, of CO_2 compared to that of brine.

CO_2 direct systems produce substantially more power than brine systems in hot and deep reservoirs. At a depth of 5 km and a geothermal gradient of 50 °C km^{-1}, the CO_2 direct pumped system produced between 0.7 MWe and 9.0 MWe more net power (an increase between 40% and 500%) over the brine system using R245fa as the secondary fluid (current state-of-the-art technology). The brine silica precipitation constraint limits the injection temperature to 176 °C in this case, resulting in the re-injection of useful thermal energy into the geothermal reservoir. Subsurface CO_2 is a poor solvent of minerals and, thus, does not have this constraint, which allows the underground CO_2 working fluid to capture and utilize more thermal energy.

CO_2 is a better working fluid in secondary Rankine cycles than R245fa. R245fa cycles operate with a higher thermal efficiency, but 'pinch-point' heat transfer constraints within heat exchangers limit the rate at which thermal energy can be captured from the geologic heat extraction fluid. Thus, CO_2 Rankine cycles can operate with more than 50% parasitic losses; however, they nonetheless result in higher net power output because they utilize more of the available geothermal heat. When using CO_2 as the secondary working fluid within secondary Rankine cycles, instead of R245fa, for base-case systems, net power production increases 22% and 20% for brine and CO_2 systems, respectively.

Increasing the well diameter substantially increases power production. Pressure losses within the wells are a major constraint on the fluid mass flowrate of a system, which directly affects power output in both CO_2 and brine systems. For example, for a 2.5 km deep, 35 °C km^{-1} thermal gradient, and 5×10^{-14} m^2 permeability reservoir, increasing injection and production well diameters from 0.27 m to 0.33 m to 0.41 m, which are still technologically reasonable well diameters, particularly in sedimentary or stratigraphic basin formations [62], increases direct pumped CO_2 net power production from 0.49 MWe to 0.70 MWe (+42%) to 0.93 MWe (+33%), respectively, resulting in a 90% overall increase in power by increasing diameter from 0.27 m to 0.41 m. For comparison, typical oil-and-gas well diameters (0.14 m) do not produce significant amounts of power in any configuration simulated, but were used in previous CPG studies [30]. It is, thus, imperative that power

output sensitivity to well diameter is considered in geothermal power production research and implementation.

This study focused on the comparison of electrical power production values of CO_2-Plume Geothermal (CPG) and brine geothermal systems for a given set of geologic and operating conditions. Future research will consider economic factors such as capital cost which also affects the design and operation of geothermal power production systems.

5. Nomenclature

Nomenclature for these simulations is provided in Table 3.

Disclaimer

Drs. Randolph and Saar have a significant financial interest, and Dr. Saar has a business interest, in TerraCOH Inc., a company that may commercially benefit from the results of this research. The University of Minnesota has the right to receive royalty income under the terms of a license agreement with TerraCOH Inc. These relationships have been reviewed and managed by the University of Minnesota in accordance with its conflict of interest policies.

Acknowledgements

Funding from a National Science Foundation (NSF) Sustainable Energy Pathways (SEP) Program Grant (1230691) is gratefully acknowledged. We would also like to thank the Initiative for Renewable Energy and the Environment (IREE), a signature program of the Institute on the Environment (IonE) at the University of Minnesota (UMN), for initial seed funding. M.O.S. thanks the George and Orpha Gibson endowment for its support of the Hydrogeology and Geofluids Research Group. Any opinions, findings, conclusions, or recommendations in this material are those of the authors and do not necessarily reflect the views of the NSF, IREE, IonE, or UMN.

Appendix A. Supplementary material

Supplementary data associated with this article can be found, in the online version, at http://dx.doi.org/10.1016/j.apenergy.2014.11.043.

References

[1] Massachusetts Institute of Technology (MIT), The future of geothermal energy: impact of enhanced geothermal systems (EGS) on the United States in the 21st century; 2006. <www.eere.energy.gov/geothermal/future_geothermal.html>.
[2] National Renewable Energy Laboratory (NREL), Geothermal power generation: current and planned nameplate capacity (MW) by state; 2014. <http://www.nrel.gov/gis/geothermal.html>.
[3] Beckers KF, Lukawski MZ, Anderson BJ, Moore MC, Tester JW. Levelized costs of electricity and direct-use heat from enhanced geothermal systems. J Renew Sustain Energy 2014;6. http://dx.doi.org/10.1063/1.4865575.
[4] Majer EL, Baria R, Stark M, Oates S, Bommer J, Smith B, et al. Induced seismicity associated with enhanced geothermal systems. Geothermics 2007;36:185–222.
[5] Brown D. A hot dry rock geothermal energy concept utilizing supercritical CO_2 instead of water. In: Proceedings of the twenty-fifth workshop on geothermal reservoir engineering, Stanford, California: Stanford University; January 24–26, 2000.
[6] Pruess K. Enhanced geothermal systems (EGS) using CO_2 as working fluid—a novel approach for generating renewable energy with simultaneous sequestration of carbon. Geothermics 2006;35:351–67.
[7] Adams BM, Kuehn TH, Bielicki JM, Randolph JB, Saar MO. On the importance of the thermosiphon effect in CPG (CO_2 plume geothermal) power systems. Energy 2014;69:409–18. http://dx.doi.org/10.1016/j.energy.2014.03.032.
[8] Luhmann AJ, Kong XZ, Tutolo BM, Garapati N, Bagley BC, Saar MO, et al. Experimental dissolution of dolomite by CO_2-charged brine at 100 °C and 150 bar: evolution of porosity, permeability, and reactive surface area. Chem Geol 2014;380:145–60.
[9] Tutolo, BM, Schaen, AT, Saar, MO, Seyfried Jr., WE. Implications of the redissociation phenomenon for mineral-buffered fluids and aqueous species transport at elevated temperatures and pressures. Special Issue in Applied Geochemistry; in press
[10] Randolph JB, Saar MO. Coupling geothermal energy capture with carbon dioxide sequestration in naturally permeable, porous geologic formations: a comparison with enhanced geothermal systems. Geotherm Res Council Trans 2010;34:433–7.
[11] Randolph JB, Saar MO. Combining geothermal energy capture with geologic carbon dioxide sequestration. Geophys Res Lett 2011;38:L10401. http://dx.doi.org/10.1029/2011GL047265.
[12] Saar MO, Randolph JB, Kuehn TH. The regents of the University of Minnesota. Carbon dioxide-based geothermal energy generation systems and methods related thereto, U.S. Patent No. 8,316,955; Canada Patent No. 2.753.393; Other International Patents pending; 2012.
[13] Zhang L, Ezekiel J, Li D, Pei J, Ren S. Potential assessment of CO_2 injection for heat mining and geological storage in geothermal reservoirs of China. Appl Energy 2014;122:237–46.
[14] IPCC. IPCC special report on carbon dioxide capture and storage. In: Metz B, Davidson O, de Coninck HC, Loos M, Meyer LA, editors. Prepared by working group III of the intergovernmental panel on climate change. New York: Cambridge University Press; 2005.
[15] Runkel AC, Miller JF, Mckay RM, Palmer AR, Taylor JF. High-resolution sequence stratiography of lower Paleozoic sheet sandstones in central North America: the role of special conditions of cratonic interiors in development of stratal architecture. Geol Soc Am Bull 2007;119:860–81.
[16] Coleman JL, Cahan SM. Preliminary catalog of the sedimentary basins of the United States: U.S. geological survey open-file report 2012–1111; 2012. <http://pubs.usgs.gov/of/2012/1111/>.
[17] Eccles JK, Pratson L. A "carbonshed" assessment of small- vs. large-scale CCS deployment in the continental US. Appl Energy 2014;113:352–61.
[18] Procesi M, Cantucci B, Buttinelli M, Armezzani G, Quattrocchi F, Boschi E. Strategic use of the underground in an energy mix plan: synergies among CO_2, CH_4 geological storage and geothermal energy. Latium Region case study (Central Italy). Appl Energy 2013;110:104–31.
[19] Global CCS Institute, The global status of CCS; 2013. <http://www.globalccsinstitute.com/publications/global-status-ccs-2013>.
[20] Randolph JB, Saar MO. Coupling carbon dioxide sequestration with geothermal energy capture in naturally permeable, porous geologic formations: implications for CO_2 sequestration. Energy Procedia 2011;4:2206–13.
[21] Carroll S, Stillman G. Assessment of key physical and chemical research findings for the use of CO_2 as a heat exchanging fluid for geothermal energy production. In: Proceedings of the thirty-ninth workshop on geothermal reservoir engineering, Stanford, California: Stanford University; February 24–26, 2014.
[22] Quattrocchi F, Boschi E, Spena A, Buttinelli M, Cantucci B, Procesi M. Synergic and conflicting issues in planning underground use to produce energy in densely populated countries, as Italy: geological storage of CO_2, natural gas, geothermics and nuclear waste disposal. Appl Energy 2013;101:393–412.
[23] Atrens AD, Gurgenci H, Rudolph V. CO_2 thermosiphon for competitive geothermal power generation. Energy Fuels 2009;23:553–7.
[24] Atrens AD, Gurgenci H, Rudolph V. Electricity generation using a carbon-dioxide thermosiphon. Geothermics 2010;39:161–9.
[25] Atrens A, Gurgenci H, Rudolph V. Economic optimization of a CO_2-based EGS power plant. Energy Fuels 2011;25:3765–75.
[26] Randolph JB, Saar MO. Impact of reservoir permeability on the choice of subsurface geothermal heat exchange fluid: CO_2 versus water and native brine. Geotherm Resour Council Trans 2011;35:521–6.
[27] Buscheck TA, Sun Y, Chen M, Hao Y, Wolery TJ, Bourcier WL, et al. Active CO_2 reservoir management for carbon storage: analysis of operational strategies to relieve pressure buildup and improve injectivity. Int J Greenhouse Gas Control 2012;6:230–45.
[28] Buscheck TA, Bielicki JM, Randolph JB, Chen M, Hao Y, Edmunds TA, Adams B, Sun Y. Multi-fluid geothermal energy systems in stratigraphic reservoirs: using brine, N_2, and CO_2 for dispatchable renewable power generation and bulk energy storage (No. LLNL-CONF-650283). In: Proceedings of the thirty-ninth workshop on geothermal reservoir engineering, Stanford, California: Stanford University; February 24–26, 2014.
[29] Janke B, Kuehn TH. Geothermal power cycle analysis for commercial applicability using sequestered supercritical CO_2 as a heat transfer or working fluid. In: Proceedings of the ASME 2011 5th international conference on energy sustainability; Aug 7–10, 2011.
[30] Pan L, Freifeld B, Doughty C, Zakem S, Sheu M, Cutright B, et al. Fully coupled wellbore-reservoir modeling of geothermal heat extraction using CO_2 as the working fluid. Geothermics 2015;53:100–13.
[31] Pruess K. The TOUGH codes — a family of simulation tools for multiphase flow and transport processes in permeable media. Vadose Zone J 2004;3:738–46.
[32] Pruess K. ECO2N: a TOUGH2 fluid property module for mixtures of water, NaCl, and CO_2. Rep. LBNL-57952, Berkeley: Lawrence Berkeley National Laboratory; 2005.
[33] Span R, Wagner W. A new equation of state for carbon dioxide covering the fluid region from the triple-point temperature to 1100 K at pressures up to 800 MPa. J Phys Chem Ref Data 1996;25:1509–96.
[34] Pollack HN, Hurter SJ, Johnson JR. Heat flow from the earth's interior: analysis of the global data set. Rev Geophys 1993;31:267–80.

[35] Global CCS Institute, The global status of CCS; 2012. <http://www.globalccsinstitute.com/publications/global-status-ccs-2012>.
[36] Frailey S, Damico J, Leetaru H. Reservoir characterization of the Mt. Simon Sandstone, Illinois Basin, USA. Energy Procedia 2011;4:5487–94.
[37] Finley R. An assessment of geologic carbon sequestration options in the Illinois basin—final report; 2005. <http://www.sequestration.org/resources/reports.html>.
[38] Sanyal S, Butler S. An analysis of power generation prospects from enhanced geothermal systems. In: Proceedings, world geothermal congress 2005, Antalya, Turkey; 24–29 April 2005.
[39] Garapati N, Randolph JB, Saar MO. Brine displacement by CO_2, energy extraction rates, and lifespan of a CO_2-limited, CO_2 Plume Geothermal system with a horizontal production well. Geothermics; in press
[40] Kong XZ, Saar MO. Numerical study of the effects of permeability heterogeneity on density-driven convective mixing during CO_2 dissolution storage. Int J Greenhouse Gas Control 2013;19:160–73.
[41] Meng Q, Jiang X. Numerical analyses of the solubility trapping of CO_2 storage in geological formations. Appl Energy 2014;130:581–91.
[42] Borgia A, Pruess K, Kneafsey TJ, Oldenburg CM, Pan L. Numerical simulation of salt precipitation in the fractures of a CO_2-enhanced geothermal system. Geothermics 2012;44:13–22.
[43] Oldenburg CM, Stevens SH, Benson SM. Economic feasibility of carbon sequestration with enhanced gas recovery (CSEGR). Energy 2004;29:1413–22.
[44] Pruess K, Moridis G, Oldenburg, C. TOUGH2 user's guide, version 2.0. Report LBNL-43134, Berkeley: Lawrence Berkeley National Laboratory; 1999.
[45] Darcy H. Les fountaines publiques de la Ville de Dijon [The public fountains of the city of Dijon]. Paris: Dalmont; 1856.
[46] Luo F, Xu RN, Jiang PX. Numerical investigation of the influence of vertical permeability heterogeneity in stratified formation and of injection/production well perforation placement on CO_2 geological storage with enhanced CH_4 recovery. Appl Energy 2013;102:1314–23.
[47] Driesner T. The system H_2O–NaCl. Part II: Correlations for molar volume, enthalpy, and isobaric heat capacity from 0 to 1000 °C, 1 to 5000 bar, and 0 to 1 XNaCl. Geochimi Cosmochim Acta 2007;71:4902–19.
[48] Haar L, Gallagher JS, Kell GS. NBS-NRC steam tables: thermodynamic and transport properties and computer programs for vapor and liquid states of water in SI units. Hemisphere; 1984.
[49] Randolph JB, Adams BM, Kuehn TH, Saar MO. Wellbore heat transfer in CO_2-based geothermal systems. Geotherm Resour Council Trans 2012;36:549–54.
[50] Pruess K, Azaraoul M. On the feasibility of using supercritical CO_2 as heat transmission fluid in an engineered hot dry rock geothermal system. In: Proceedings, thirty-first workshop on geothermal reservoir engineering, Stanford, California: Stanford University; January 30-February 1, 2006.
[51] Moody L. Friction factors for pipe flow. Trans ASME 1944:671–84.
[52] Wang JL, Zhao L, Wang XD. An experimental study on the recuperative low temperature solar Rankine cycle using R245fa. Appl Energy 2012;94:34–40.
[53] Yin H, Sabau AS, Conklin JC, McFarlane J, Qualls AL. Mixtures of SF_6–CO_2 as working fluids for geothermal power plants. Appl Energy 2013;106:243–53.
[54] Ghasemi H, Sheu E, Tizzanini A, Paci M, Mitsos A. Hybird solar-geothermal power generation: Optimal retrofitting. Appl Energy 2014;131:158–70.
[55] Adams BM, Kuehn TH, Randolph JB, Saar MO. The reduced pumping power requirements from increasing the injection well fluid density. Geotherm Resour Council Trans 2013;37:667–72.
[56] Goulds, Goulds VIT vertical industrial turbine pumps; 2013 <http://www.gouldspumps.com/Products/VIT/>.
[57] DiPippo R. A simplified method for estimating the silica scaling potential in geothermal power plants. Geotherm Resour Council Bull 1985.
[58] Maraver D, Royo J, Lemort V, Quoilin S. Systematic optimization of subcritical and transcritical organic rankine cycles (ORCs) constrained by technical parameters in multiple applications. Appl Energy 2014;117:11–29.
[59] Chen H, Goswami DY, Rahman MM, Stefanakos EK. Energetic and exergetic analysis of CO_2-and R32-based transcritical Rankine cycles for low-grade heat conversion. Appl Energy 2011;88:2802–8.
[60] Shengjun Z, Huaixin W, Tao G. Performance comparison and parametric optimization of subcritical Organic Rankine Cycle (ORC) and transcritical power cycle system for low-temperature geothermal power generation. Appl Energy 2011;88:2740–54.
[61] Toffolo A, Lazzaretto A, Manente G, Paci M. A multi-criteria approach for the optimal selection of working fluid and design parameters in organic rankine cycle systems. Appl Energy 2014;121:219–32.
[62] United States Department of Energy (DOE), Geothermal electricity technology evaluation model (GETEM); 2012. <http://energy.gov/eere/geothermal/geothermal-electricity-technology-evaluation-model>.
[63] Freifeld B, Zakim S, Pan L, Cutright B, Sheu M, Doughty C, et al. Geothermal energy production coupled with CCS: a field demonstration at the SECARB Cranfield Site, Cranfield, Mississippi, USA. Energy Procedia 2013;37:6595–603.
[64] Nathenson M, Guffanti M. Geothermal gradients in the continuous United States. J Geophyis Res 1985;93:6437–50.
[65] Sauret E, Gu Y. Three-dimensional off-design numerical analysis of an organic rankine cycle radial-inflow turbine. Appl Energy 2014;135:202–11.
[66] Farshad F, Rieke H. Surface-roughness design values for modern pipes. SPE Drill Complet 2006:212–5.